

Title	Coastal infrastructure operativity against flooding - A methodology
Authors	Rodriguez-Delgado, Cristobal;Bergillos, Rafael J.;Iglesias, Gregorio
Publication date	2020-02-21
Original Citation	Rodriguez-Delgado, C., Bergillos, R. J. and Iglesias, G. (2020) 'Coastal infrastructure operativity against flooding - A methodology', Science of the Total Environment, 719, 137452 (11pp). doi: 10.1016/j.scitotenv.2020.137452
Type of publication	Article (peer-reviewed)
Link to publisher's version	10.1016/j.scitotenv.2020.137452
Rights	© 2020, Elsevier B.V. All rights reserved. This manuscript version is made available under the CC BY-NC-ND 4.0 license. - https://creativecommons.org/licenses/by-nc-nd/4.0/
Download date	2025-07-03 23:52:32
Item downloaded from	https://hdl.handle.net/10468/9907



UCC

University College Cork, Ireland
 Coláiste na hOllscoile Corcaigh

Coastal infrastructure operativity against flooding – a methodology

Cristobal Rodriguez-Delgado^{a,b}, Rafael J. Bergillos^{c,*}, Gregorio Iglesias^{d,a}

^a*School of Engineering, University of Plymouth, Plymouth PL4 8AA, UK*

^b*PROES Consultores, Calle San Germán 39, 28020 Madrid, Spain*

^c*Hydraulic Engineering Area, Department of Agronomy, University of Cordoba, Rabanales Campus, Leonardo da Vinci Building, 14071 Córdoba, Spain*

^d*MaREI, Environmental Research Institute & School of Engineering, University College Cork, College Road, Cork, Ireland*

Abstract

The operativity of the transport infrastructures and urban developments protected by coastal structures is conditioned by flooding events and the resulting wave overtopping. This work presents a methodology to assess the operational conditions of infrastructures located in coastal areas based on the combination of advanced statistical techniques, laboratory experiments and state-of-the-art numerical models properly validated. It is applied to a case study in the SW coast of England, the railway seawall at Dawlish, which was subjected to recurrent wave overtopping until its dramatic collapse in February 2014. To quantify the increase in overtopping discharges with wave height and water level, we define an *ad hoc* variable, the *effective overtopping forcing*, which explains 98% of the variability of the overtopping discharge. The return periods associated to the operational thresholds for coastal structures protecting people and railways are also obtained. The proposed methodology enables the assessment of the overtopping discharge induced by a given sea state and, thus, check if a coastal infrastructure will be or not operational under any expected marine condition. This innovative methodology can also be used to analyse the flooding event consequences on urban areas protected by coastal infrastructures.

*Corresponding author.
E-mail address: rafael.bergillos@uco.es

Keywords: Coastal flooding; Seawall; Operationality; Statistics; Laboratory experiments; Numerical modelling

1. Introduction

Coastal flooding is one of the environmental hazards with the greatest potential impact on human activity [1–6]. Flooding typically occur as a result of wave overtopping of coastal structures [7–9]. These flooding events will be more frequent and severe in the next decades due the rise in sea level and other consequences of climate change [10–15]. When coastal structures protect transport infrastructure (railway lines, roads, etc.), wave overtopping can disrupt the chain of transport, with strong repercussions for the society and economy of the region. Some recent studies have dealt with the impacts of wave overtopping on transport infrastructure (e.g., [16] or [17]). Wave overtopping has also been studied in connection with flood-control structures [18–22], rockfill dams [23, 24] and coastal structures [25, 26].

Coastal structures are designed to fulfil specific social, economic and/or environmental functions. They often have a multi-functional nature [27]. In the case of seawalls, their primary function is to protect urban areas and transport infrastructure against coastal flooding [28–36]. The operativity of seawalls is mainly conditioned by wave overtopping. Thus, it is essential to predict overtopping discharges accurately [37–40].

The design conditions for a coastal structure are commonly obtained through extreme value analysis of long-term data series, in which the design significant wave height is calculated for a prescribed return period. In the case of wave overtopping, there is another factor of utmost importance: the water level, which is determined by the astronomical tide and storm surge. On top of that, the rise in sea level will have an important impact on return periods, giving even more importance to the water level at the toe of the coastal structures. Multivariate extreme value analysis must be applied, therefore, to establish the joint probability distribution of water level and wave height [41–43].

28 Wave overtopping has been traditionally assessed by means of physical mod-
29 elling. Laboratory experiments have provided valuable data [44–51]. Based
30 on these data, design equations have been derived [52–54] and neural network
31 techniques have been applied [55–58]. However, structures with non-standard
32 geometries require *ad hoc* tests [59]. As this may not always be possible for
33 reasons of cost and time, especially in order to assess the operativity of an
34 existing structure, numerical modelling of wave overtopping is becoming ever
35 more popular. Several numerical models have been developed so far to deter-
36 mine overtopping rates on coastal structures [60–63]. Among them, CFD (Com-
37 putational Fluid Dynamics) models, based on the RANS (Reynolds-Averaged
38 Navier-Stokes) equations and the VOF (Volume-of-Fluid) method [64] for cap-
39 turing the free surface, are able to simulate the non-linearities in wave-structure
40 interaction, which renders them particularly attractive.

41 There is very little knowledge concerning the effects of wave overtopping on
42 transport systems in the lee of seawalls or breakwaters. [65] studied the effects
43 of wave overtopping jets on pedestrians and vehicles based on physical mod-
44 elling and suggested some guidelines for operational purposes. More recently,
45 these guidelines have been updated in [66], including operational thresholds for
46 railways, highways, roads and people.

47 In this paper, a novel methodology to assess the operational conditions of
48 infrastructures against coastal flooding is proposed. It is based on the combi-
49 nation of multivariate extreme analysis and numerical modelling applications
50 (Section 2). The methodology is applied to a study case: the Dawlish seawall,
51 in the UK (Section 3). This infrastructure is infamous for its failure during
52 the storms of February 2014 and the consequent disruption to the all-important
53 railway line connecting SW England with the rest of the country.

54 **2. Description of the methodology**

55 The methodology proposed in this work to quantify the operational condi-
56 tions is summarized in Fig. 1. Based on the deep-water water level (η) and

57 significant wave height (H_{s0}) data at a given study area, an extreme value anal-
 58 ysis for both variables is first required to obtain the joint probability distribution
 59 (Section 2.1). To characterize the whole universe of water level and significant
 60 wave height combinations, a mesh is created based on the selection of N pairs
 61 of values (η , H_{s0}). The sea states selected are propagated from deep water to
 62 the location of the structure using a numerical wave propagation model (Section
 63 2.2). The local wave conditions thus obtained are employed as input conditions
 64 to apply a CFD model (Section 2.3), which allows computing wave overtop-
 65 ping discharges. Based on these overtopping discharge values, the operational
 66 conditions of the infrastructure against coastal flooding are assessed (Section
 67 2.4).

68 *2.1. Assessment of extreme values and joint probability*

69 In order to assess the risks associated with wave overtopping, it is crucial
 70 to determine the joint probability of extreme water levels and wave heights. In
 71 this work, the novel statistical dependence methodology for compound events
 72 developed by the Joint Research Centre of the European Commission [67] is
 73 used.

74 For any combination of water level and significant wave height, the joint
 75 return period of occurrence is defined as

$$T_{X,Y} = \sqrt{\frac{T_x \cdot T_y}{\chi^2}}, \quad (1)$$

76 where T_x and T_y are the return periods of the water level and significant wave
 77 height, respectively. The parameter χ is the dependence measure, calculated as

$$\chi(u) = 2 - \frac{\ln P(U \leq u, V \leq u)}{\ln P(U \leq u)}, \quad (2)$$

78 where u is a common threshold selected as the 99th percentile of the signif-
 79 icant wave height from the wave dataset and of the water level from the water
 80 level record. This dependence coefficient varies between 0 (no correlation) and
 81 1 (total correlation).

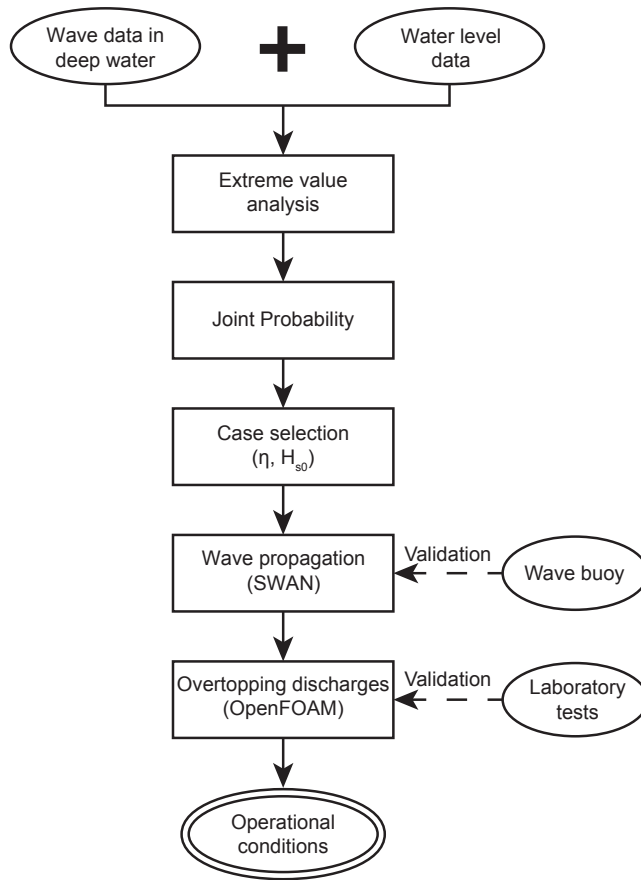


Figure 1: Flow chart of the methodology proposed in this work.

82 *2.2. Numerical modelling of wave propagation*

83 The sea states in deep water are propagated toward the location of the outer
 84 boundary of the CFD model by means of SWAN, a 3rd generation spectral
 85 wave model [68, 69]. This model reproduces the main processes related to
 86 wave propagation, such as refraction, shoaling, breaking as well as diffraction,
 87 transmission and reflection induced by obstacles. The SWAN model has been
 88 used over the past few years for a wide range of coastal engineering applications
 89 [70–86].

90 *2.3. Numerical modelling of wave overtopping discharge*

91 In order to obtain the wave overtopping discharge for each one of the N
92 combinations (η, H_{s0}) selected and propagated with SWAN, the use of a CFD
93 numerical model is required. OpenFOAM[®] [87] was chosen due to its open-
94 source character along with its wide and active community of users.

95 *2.4. Assessment of operational conditions*

96 The operational conditions of a coastal infrastructure are defined by its func-
97 tionality. In the case of seawalls, the main goal of the structure is generally to
98 protect the transport infrastructures and people in the lee of the seawalls. Euro-
99 top [66] defines some limitations to overtopping discharges in terms of structural
100 design and, more specifically for structures protecting transport infrastructures
101 and people.

102 **3. Application of the methodology to a case study**

103 *3.1. Description of the study site*

104 The study site, Dawlish, is located in the Lyme Bay (SW England, UK),
105 in the western margin of the English Channel (Fig. 2). The Dawlish seawall
106 protects the railway line from London to Penzance, which was opened to the
107 traffic in 1846 and designed by I.K. Brunel. This line is the only rail connection
108 between the SW of England and the rest of the country. The section of the
109 line between Teignmouth and Dawlish, which connects the cities of Plymouth
110 and Exeter, follows the shoreline and is protected from wave action by a nearly
111 vertical seawall (the aforementioned Dawlish seawall). This section has suffered
112 multiple disruptions throughout its history due to wave overtopping [88].

113 The storm of February 2014 is a good example of the havoc that can be
114 wreaked by natural hazards on transport infrastructure. Part of the seawall
115 collapsed under the combination of extreme waves and water levels, leaving the
116 rails dangling in the air (Fig. 3). The line stayed close to the traffic over months,
117 with serious repercussions for the region. The cross-section of the seawall varies

118 along Dawlish. To apply the methodology proposed in this paper, the section
119 corresponding to Riviera Terrace was considered (Fig. 4). This was the zone
120 that suffered most of the damage during the storm event in February 2014 (Fig.
121 3).

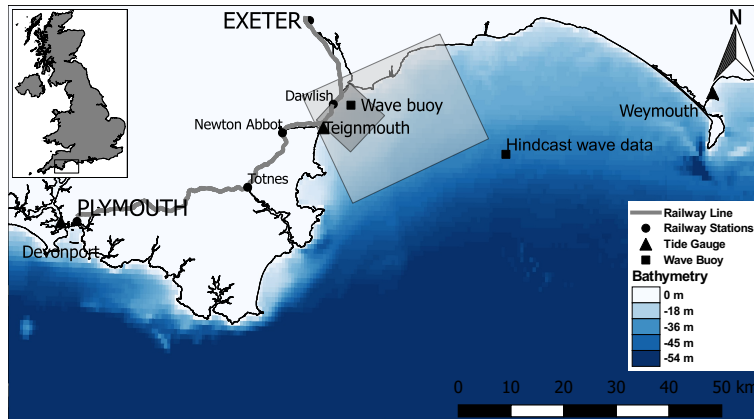


Figure 2: Location of the study area (top-left panel). The central panel shows the track of the railway line and the more important stations connected, along with the location of the tide gauges, wave buoy and hindcast data point, the grids employed in the propagation model and the bathymetry.



Figure 3: Seawall collapsed at Dawlish on 6 February 2014, with rails hanging in mid-air. Source: <http://www.geograph.org.uk/photo/3838795>. Copyright: Derek Harper, Creative Commons Licence.

122 The wave regime at the study area is characterised by the joint influence
123 of North Atlantic swells with SW mean direction and locally generated waves.
124 The 50%, 90% and 99% non-exceed deep-water significant wave heights are 0.9
125 m, 2.1 m and 3.5 m, respectively. The maximum observed value of significant
126 wave height is 10.4 m, corresponding to the storm of February 2014. The tidal
127 range at Teignmouth is 4.9 m.

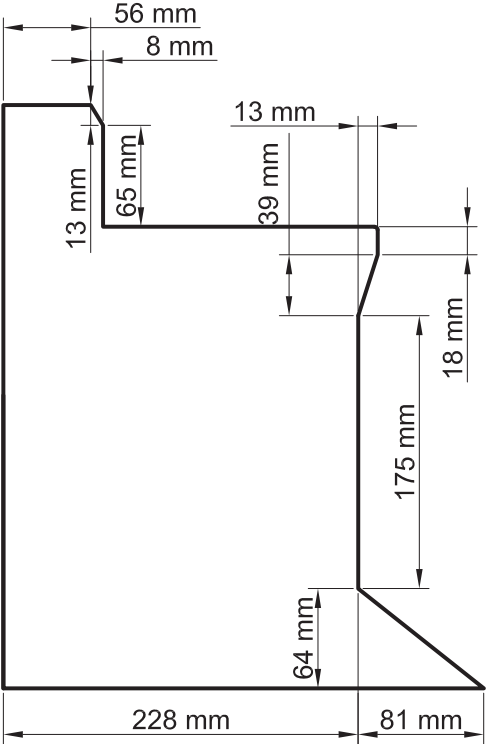


Figure 4: Cross-section of the Dawlish seawall at a 1:20 scale.

128 *3.2. Extreme values*

129 The wave data used in this work were obtained through the WAM North
130 Atlantic hindcast wave model (Fig. 2). This dataset contains a 50-year time
131 series of hourly wave hindcast data including significant wave heights, spectral
132 peak periods, and mean incoming wave directions. Based on these data, return
133 periods for extreme wave height values were assessed using the r-largest method
134 [89]. The five maximum wave height values per annum were selected over the
135 50-year time series, and a EV (Generalised Extreme Value) distribution was
136 fitted.

137 The tide gauge nearest to Dawlish is situated at Teignmouth, 6 km away.
138 Its record only comprises 6 years of data, an insufficient length to assess return
139 periods properly. To extend the record, the Inverse Distance Weighting (IDW)
140 method was applied using the tide gauges at Devonport and Weymouth (Fig.
141 2). The distance coefficients for the IDW method were calibrated and validated
142 using the data of the Teignmouth record, and a correlation coefficient $R = 0.99$
143 was obtained. In this way, the record was extended to 26 years. Likewise,
144 the r-largest method was employed to obtain the return periods associated to
145 extreme water levels, using again the five annual maxima per year and the GEV
146 distribution.

147 The diagnostic plots of the GEV distribution fitted to the five maximum
148 values per year of significant wave height are shown in Fig. 5. The GEV
149 is defined by three parameters: scale (σ), shape (k) and location (μ). The
150 value of k characterizes the tail behaviour of the function and divides the GEV
151 distribution into three subtypes: Type I ($k = 0$), Type II ($k > 0$) and Type III
152 ($k < 0$). The best fit was obtained with $k = 0.0518$ (Fig. 5c). This results in
153 a Type II GEV function, with positive first and second derivatives (Fig. 5c),
154 implying that H_s increases with the return period indefinitely. The divergence
155 of the tail of the distribution accounts for the probability of heavy storms, such
156 as the infamous February 2014 gale, which resulted in extreme wave overtopping
157 and the subsequent collapse of the Dawlish seawall.

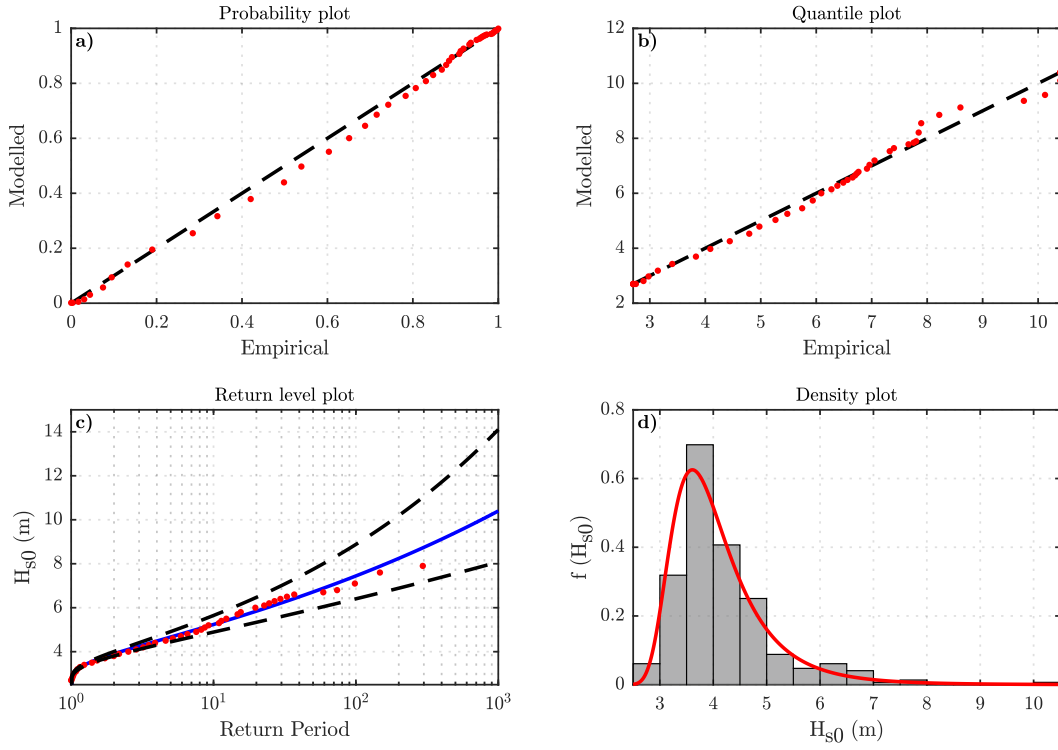


Figure 5: Diagnostics plots for the GEV distribution fitted to the significant wave heights in deep water (H_{s0}).

158 On the other hand, the diagnostic plots of the GEV distribution fitted to
 159 the water level data at Teignmouth (Fig. 6) have an optimum shape parameter
 160 equal to $k = -0.13$. This results in a Type III GEV distribution and a different
 161 tail behaviour, with a negative second derivative that hints at an asymptotic
 162 tendency for large values of the return period (Fig. 6c). The water level is
 163 controlled by the astronomical tide and the meteorological influences which
 164 govern the storm surge (atmospheric pressure and wind). The astronomical tide
 165 is a deterministic nature and the influence of storm surge can only go so far.
 166 For this reason, the tail behaviour of the GEV distribution is clearly different
 167 in the case of water level.

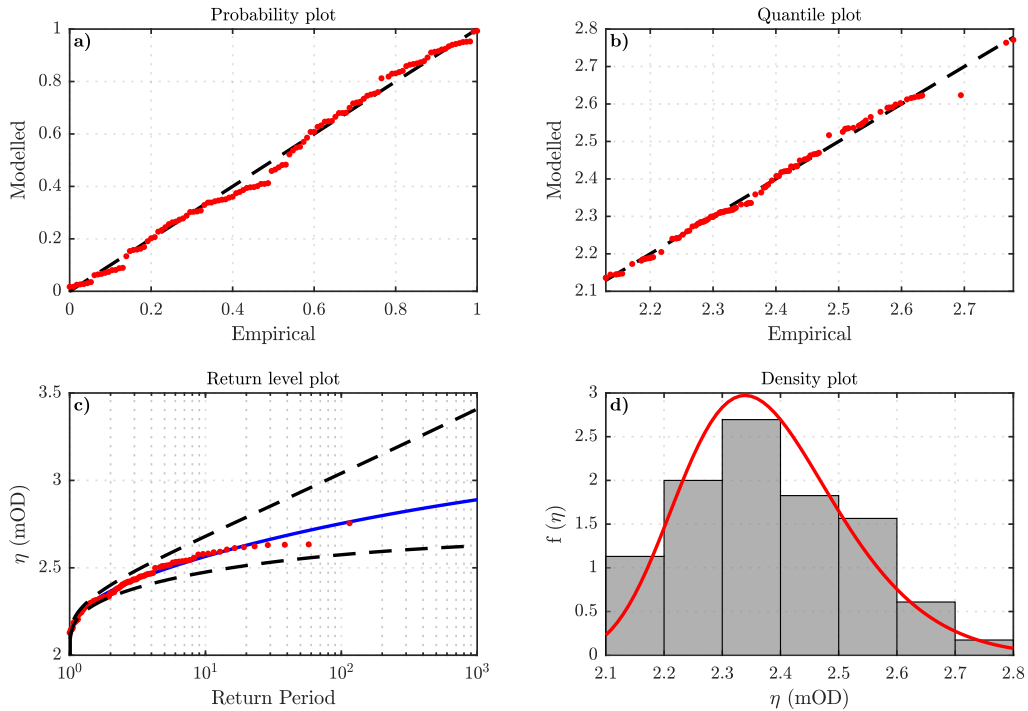


Figure 6: Diagnostics plots for the GEV distribution fitted to the water levels (η).

168 *3.3. Joint probability*

169 The joint probability analysis yields a dependence coefficient $\chi = 0.57$, which
 170 implies a strong correlation between extreme water levels and wave heights. The
 171 outputs of the analysis are the joint probability curves for joint return period
 172 values of 5, 10, 25, 50, 100, 250 and 500 years, i.e. the isolines of joint return
 173 period in the (η, H_{s0}) plane (Fig. 7). In this way, the area between the isoline,
 174 the x-axis and the y-axis may be assumed as a measurement of the number of
 175 pairs (η, H_{s0}) whose joint return period is equal or lower than the value of the
 176 isoline.

177 Therefore, a comparison between the area under the isoline of joint return
 178 period (calculated considering the water level and significant wave height as
 179 independent variables) and that obtained using the dependence coefficient, leads
 180 to an estimation of the number of cases whose probability of occurrence would

181 be underrated with traditional independent analysis. The cases with a longer
 182 joint return period are the most underestimated. The areas under the 500-year,
 183 250-year and 100-year isolines increase by 29.7%, 26.7% and 22.5%, respectively;
 184 whereas the increase in the area under the 5-year isoline is equal to 6.2%.

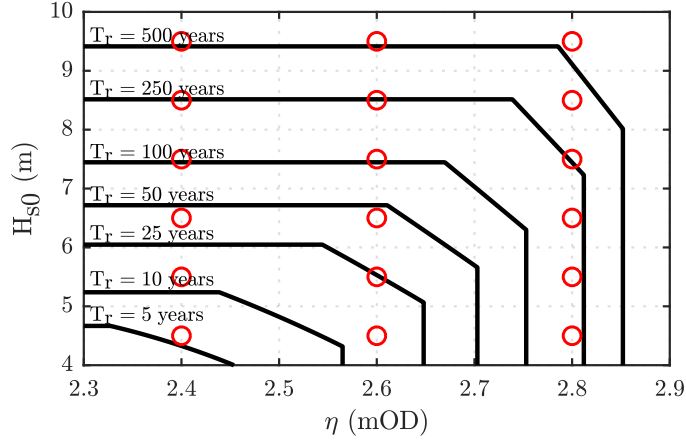


Figure 7: Isolines corresponding to return period values of 5, 10, 25, 50, 100, 250 and 500 years (black lines), and pairs (η, H_{s0}) analysed (red dots).

185 3.4. Wave propagation

186 The computational domain used to perform the wave propagation with
 187 SWAN is divided into two grids (Fig. 2): (i) a coarse grid composed by 207×207
 188 rectangular cells of 130×105 m, covering the region between 40 m water depths
 189 and the coastline; and (ii) a nested grid composed by 406×406 rectangular cells
 190 of 23×22 m, covering the shallow water area, with maximum depths of 23 m.
 191 The bathymetry was obtained from the UKHO INSPIRE portal. The frequency
 192 space, between 0.03 and 0.4 Hz, was divided into 32 bins, while the directional
 193 space covered 360° with a resolution of 5° (72 directional bins).

194 The SWAN model was calibrated and validated using data from the coastal
 195 wave buoy located at Dawlish (Fig. 2), managed by the Channel Coastal Ob-
 196 servatory. The length of this dataset is 6 years of hourly wave data, including
 197 significant wave height, spectral peak period, and mean incoming wave direc-

198 tion. The calibration period, from 1 February 2014 to 28 February 2014, was
 199 chosen for its extreme wave conditions. The SWAN model was forced using the
 200 WAM data and taking into account the following processes: bottom friction,
 201 non-linear triad interactions, refraction, diffraction, whitecapping and depth-
 202 induced wave breaking. The results of the validation are depicted in Fig. 8.
 203 The correlation coefficient between the results of the model and the wave buoy
 204 observations is $R = 0.94$, with a RMSE= 0.25 m.

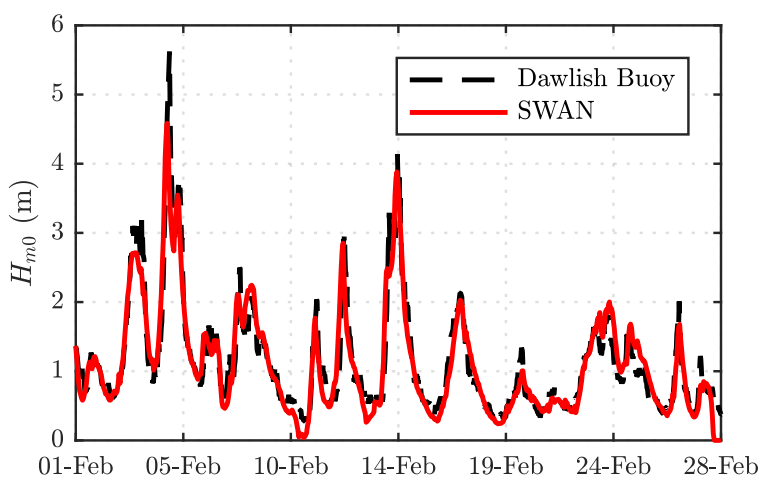


Figure 8: Comparison between measured and modelled significant wave height time series in February 2014 at the location of the wave buoy (Fig. 2).

205 3.5. Wave overtopping

206 3.5.1. Laboratory experiments

207 The physical model of the seawall was built in marine plywood at a 1:20
 208 scale (Fig. 4). The tests were carried out in the COAST laboratory at the
 209 University of Plymouth, in a 0.6-m-wide and 35-m-long wave flume (Fig. 9).
 210 The wave paddle is equipped with an active wave absorption control system.
 211 The toe of the model was situated at a distance of 23.88 m from the paddle. In
 212 front of the model, a ramp was located to reproduce the bathymetry; whereas
 213 the still water level was set at 0.5 m. Eight resistive wave gauges were used
 214 during the experiments (Fig. 9). Seven wave gauges (WG1–WG7) were placed

215 between the wave paddle and the model, and an additional wave gauge (WG8)
 216 was located behind the model to measure the overtopping volume.

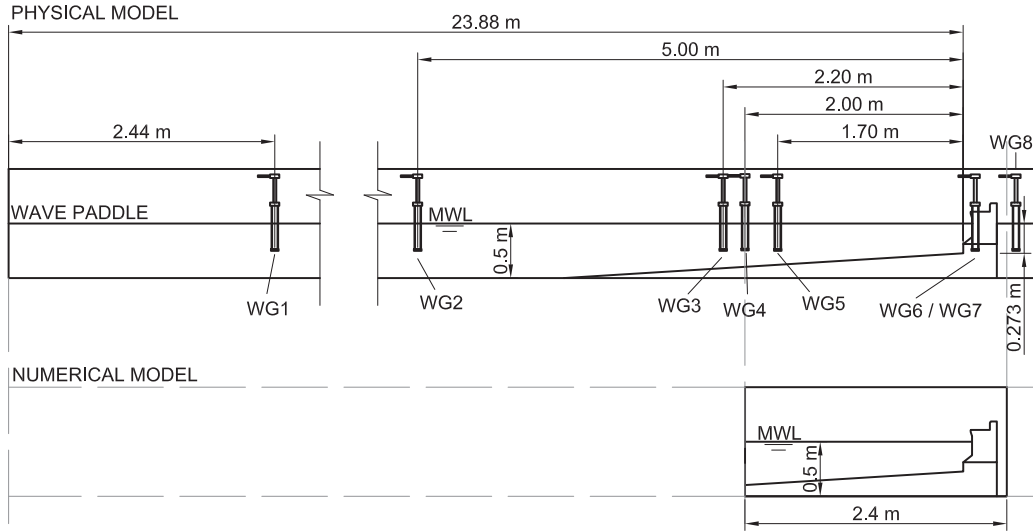


Figure 9: Physical and numerical set-ups.

217 Eighteen irregular wave tests were carried out, covering significant wave
 218 height values between 1.7 m and 4.4 m, and peak period values varying from
 219 7 s to 13 s (prototype scale). The incident and reflected wave spectra were
 220 separated through a least-squares method using the measurements of three wave
 221 gauges (WG 3, WG 4 and WG 5). These data were employed to validate the
 222 CFD model (Section 3.5.2).

223 3.5.2. Set-up and validation of OpenFOAM[®]

224 The computational domain spans a total length of 2.4 m, between the posi-
 225 tion of WG4 and the rear of the model (Fig. 9). Thus, the computational cost
 226 was reduced without compromising the accuracy of the simulations. The inci-
 227 dent wave spectra at the upstream boundary (WG4) were obtained by means
 228 of the aforementioned incident-reflected wave analysis. The height of the com-
 229 putational domain was 1.2 m and, as there is no directionality in the irregular
 230 waves generated, the width of the computational domain was covered by a cell.

231 The initial meshing of the computational domain was generated by the
 232 “blockMesh” utility included in OpenFOAM[®], and it was composed by rectan-
 233 gular cells of 1 x 0.5 cm. To simulate the interaction between flow and model,
 234 the ramp and the seawall were removed from the mesh using the utility “snap-
 235 pyHexMesh”, also included in OpenFOAM[®] (Fig. 10). The desired still water
 236 level was achieved setting $\alpha = 1$ (full of water) for those cells with $z \leq \eta$ and
 237 $\alpha = 0$ (full of air) for $z > \eta$, where η is the desired water level for each test.

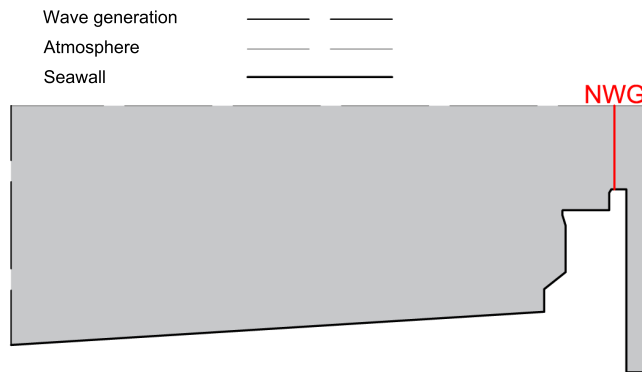


Figure 10: Computational domain, boundary conditions and numerical wave gauge (NWG) used in OpenFOAM[®].

238 The numerical tests for the validation were carried out considering the same
 239 wave conditions as the physical model experiments (Table 1), and with the same
 240 number of waves (200). Velocities and elevations of the free surface over the
 241 freeboard were determined by means of a numerical wave gauge. The correlation
 242 coefficient obtained was $R = 0.89$ (Fig. 11), presenting a greater statistical
 243 correlation for overtopping discharges below 50×10^{-3} l/s per m.

Table 1: Overtopping discharges measured in the laboratory and obtained with the numerical model [H_s : significant wave height; T_p : spectral peak period; Q_m : mean overtopping discharge measured in the laboratory; Q_n : mean overtopping discharge obtained with the numerical model].

H_s (m)	T_p (s)	Q_m (10^{-3} l/s per m)	Q_n (10^{-3} l/s per m)
0.085	2.01	0	0
0.085	2.45	1.4	0.4
0.085	2.9	0	0
0.112	1.56	1	4
0.112	2.01	3	11
0.112	2.45	14	12.7
0.112	2.9	23	13
0.14	1.56	7.4	4.1
0.14	2.01	36	69
0.14	2.45	70	109
0.14	2.9	125	100
0.166	1.56	22	24
0.166	2.01	54	52
0.166	2.45	163	203
0.166	2.9	248	179
0.194	2.01	179	83
0.194	1.56	27	16
0.221	1.56	42	28

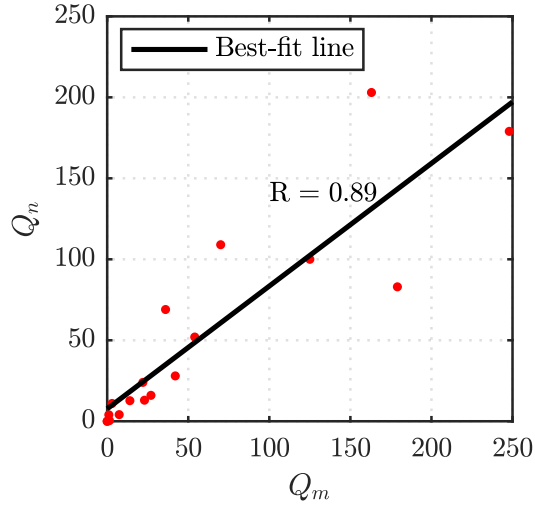


Figure 11: Scatter diagram of the mean overtopping discharges measured in the laboratory experiments (Q_m) and modelled with the CFD numerical model (Q_n). R is the correlation coefficient.

244 *3.5.3. Wave overtopping discharges*

245 Apart from water level and significant wave height, for the definition of a
 246 sea state, the spectral peak period (T_p) is required. As the objective of this
 247 work is to characterize the operational conditions of a coastal structure against
 248 extreme events (floodings), only sea states with $H_{s0} > 3$ m were considered,
 249 referred to henceforth as extreme sea states. The universe of extreme sea states
 250 in the hindcast dataset was divided into three regions based on wave steepness,
 251 H_{s0}/L_0 , where L_0 is the wavelength in deep water, which is related to the peak
 252 period as follows:

- 253 • Region I: high-steepness sea states, with $0.025 < H_{s0}/L_0$,
- 254 • Region II: mid-steepness sea states, with $0.020 < H_{s0}/L_0 < 0.025$, and
- 255 • Region III: low-steepness sea states, with $H_{s0}/L_0 < 0.020$.

256 Curves were fitted to the data in each region, defined by:

$$T_p = 3.40H_{s0}^{0.58} + 1.34, \quad (3)$$

$$T_p = 6.87H_{s0}^{0.44} - 1.67, \text{ and} \quad (4)$$

$$T_p = 2.63H_{s0}^{0.74} + 6.53. \quad (5)$$

257 Equations 3, 4 and 5 correspond to the best-fit curves of Regions I, II and
 258 III, respectively. Regions I and II show a strong correlation between H_{s0} and
 259 T_p , with $R = 0.76$ and $R = 0.92$, respectively. By contrast, Region III shows a
 260 weaker correlation, with $R = 0.38$. In any case, Regions I and II are the most
 261 interesting from the standpoint of the operativity of the seawall, since they
 262 contain the most extreme wave heights. The majority of extreme sea states
 263 come from the SW; however, these sea states can have different provenances:
 264 ocean swells propagating into the Channel or locally-generated wind waves, the
 265 latter with comparatively higher wave steepness. The division of the universe
 266 of significant wave heights and peak periods into two regions (I and II) seeks to
 267 represent these two provenances.

268 Eighteen pairs (η, H_{s0}) were defined by creating a mesh around the isolines
 269 of joint return period (Fig. 7). For each of these pairs defined, two values of the
 270 peak wave period were determined using Eqs. 3 and 4. This provided a total of
 271 36 cases for the combined numerical modelling approach (wave propagation and
 272 CFD). The results obtained with the combined numerical modelling are pre-
 273 sented in Table 2. For ten of the pairs (η, H_{s0}) tested, the discharge is greater
 274 in Region II (mid-steepness) than in Region I (high-steepness). Five pairs ex-
 275 hibit the opposite behaviour, and in the rest of cases there is no overtopping.
 276 Independently of the wave steepness region considered, the mean overtopping
 277 discharge increases with increasing water levels and significant wave heights
 278 (Fig. 12a, b). The averages of the mean overtopping discharges for constant
 279 values of η and H_{s0} are shown in Table 3.

Table 2: Results of the combined numerical models [η : water level; H_{s0} : significant wave height in deep water; T_{pI} : peak period in region I; Q_{nI} : mean overtopping discharge in Region I; T_{pII} : peak period in region II; Q_{nII} : mean overtopping discharge in Region II].

Case Id.	η (mOD)	H_{s0} (m)	T_{pI} (s)	Q_{nI} ($\text{ls}^{-1}\text{m}^{-1}$)	Case Id.	η (mOD)	H_{s0} (m)	T_{pII} (s)	Q_{nII} ($\text{ls}^{-1}\text{m}^{-1}$)
1 _I	2.4	4.5	9.5	0	1 _{II}	2.4	4.5	11.6	0
2 _I	2.4	5.5	10.5	0	2 _{II}	2.4	5.5	12.9	0.09
3 _I	2.4	6.5	11.4	0.83	3 _{II}	2.4	6.5	14.0	0.23
4 _I	2.4	7.5	12.3	1.48	4 _{II}	2.4	7.5	15.0	3.02
5 _I	2.4	8.5	13.1	3.64	5 _{II}	2.4	8.5	15.9	5.92
6 _I	2.4	9.5	13.9	9.01	6 _{II}	2.4	9.5	16.8	9.47
7 _I	2.6	4.5	9.5	0	7 _{II}	2.6	4.5	11.6	0
8 _I	2.6	5.5	10.5	0.01	8 _{II}	2.6	5.5	12.9	0.08
9 _I	2.6	6.5	11.4	1.13	9 _{II}	2.6	6.5	14.0	0.25
10 _I	2.6	7.5	12.3	2.12	10 _{II}	2.6	7.5	15.0	3.66
11 _I	2.6	8.5	13.1	5.03	11 _{II}	2.6	8.5	15.9	6.92
12 _I	2.6	9.5	13.9	12.5	12 _{II}	2.6	9.5	16.8	11.8
13 _I	2.8	4.5	9.5	0	13 _{II}	2.8	4.5	11.6	0
14 _I	2.8	5.5	10.5	0.06	14 _{II}	2.8	5.5	12.9	0.14
15 _I	2.8	6.5	11.4	1.57	15 _{II}	2.8	6.5	14.0	0.38
16 _I	2.8	7.5	12.3	2.73	16 _{II}	2.8	7.5	15.0	4.52
17 _I	2.8	8.5	13.1	6.63	17 _{II}	2.8	8.5	15.9	7.88
18 _I	2.8	9.5	13.9	16	18 _{II}	2.8	9.5	16.8	13.4

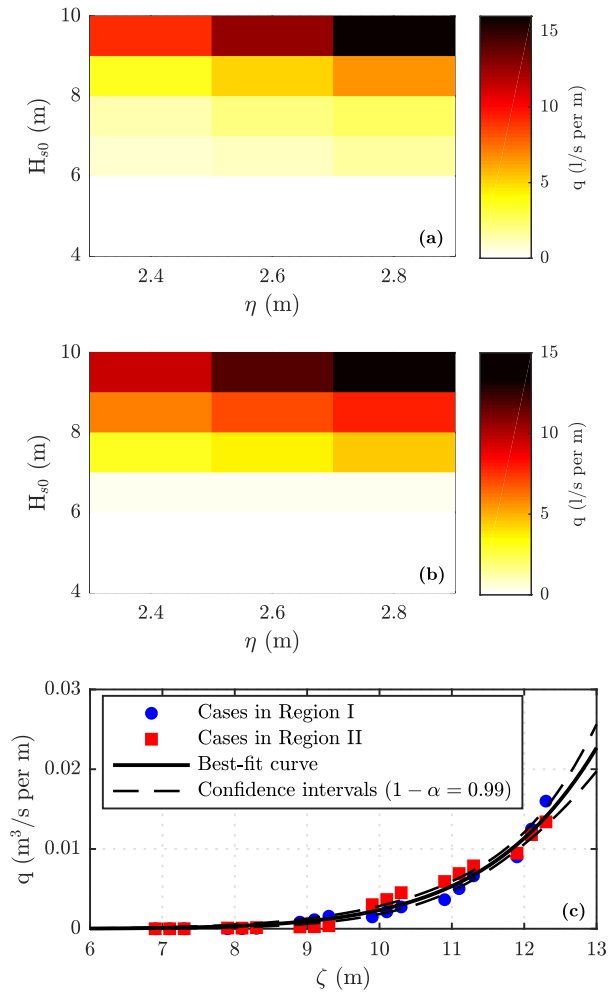


Figure 12: Mean overtopping discharges modelled for wave steepness Regions I (a) and II (b). (c) Mean overtopping discharge (q) variation as a function of the effective overtopping forcing (ζ).

Table 3: Averages of the mean overtopping discharges for constant values of water level and significant wave height in deep water [η : water level; H_{s0} : significant wave height in deep water; \bar{Q}_{nI} : average of the mean overtopping discharge in Region I; \bar{Q}_{nII} : average of the mean overtopping discharge in Region II].

	\bar{Q}_{nI}	\bar{Q}_{nII}
	($\text{ls}^{-1}\text{m}^{-1}$)	($\text{ls}^{-1}\text{m}^{-1}$)
$\eta = 2.4$ m	2.49	3.12
$\eta = 2.6$ m	3.47	3.79
$\eta = 2.8$ m	4.5	4.39
$H_{s0} = 4.5$ m	0	0
$H_{s0} = 5.5$ m	0.02	0.1
$H_{s0} = 6.5$ m	1.18	0.29
$H_{s0} = 7.5$ m	2.11	3.73
$H_{s0} = 8.5$ m	5.1	6.91
$H_{s0} = 8.5$ m	12.5	11.56

280 Having established that the mean overtopping rate is mainly driven by water
281 level and significant wave height, for the purposes of this work, we define an *ad*
282 *hoc* variable, the *effective overtopping forcing*, as

$$\zeta = \eta + H_{s0}. \quad (6)$$

283 The interest of this new variable is its capacity to predict the overtopping
284 discharge for both regions (I and II). The best-fit curve is:

$$q = k\zeta^9. \quad (7)$$

285 with q = mean overtopping discharge (m^2s^{-1}) and $k = 2.21 \times 10^{-12}$ ($\text{m}^{-7}\text{s}^{-1}$).
286 The coefficient of determination obtained with Eq. (7) is equal to 0.98, that is,
287 98% of the variability of the overtopping discharge is explained by Eq. 7. This
288 strong correlation between the *effective overtopping forcing* and the overtopping
289 discharge is also observed in Fig. 12c.

290 *3.6. Operational conditions*

291 The EurOtop [66] indicates that the threshold of overtopping discharge that
 292 limits the operational conditions on seawalls protecting a railway is overtopping
 293 discharge equal to 5 l/s per m; whereas in the case of seawalls protecting people,
 294 this limit is equal to 0.3 l/s per m. As can be observed in Table 2, eleven
 295 (twenty-two) of the thirty-six cases exceed the railway (people) threshold.

296 To better illustrate the operational conditions, Fig. 13 shows the warning
 297 level of each (η, H_{s0}) combination for both railway infrastructures and people
 298 along with different return period curves. It is observed that a certain value
 299 of mean overtopping discharge may have infinite return periods, as it can be
 300 the result of infinite (η, H_{s0}) combinations. The separation lines between the
 301 different warning levels in Fig. 13 are the isolines of the mean overtopping
 302 discharges corresponding to their specific thresholds.

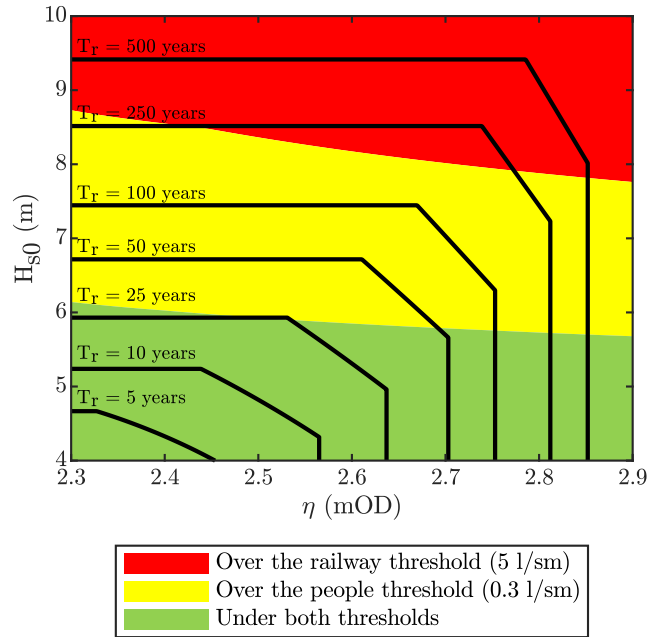


Figure 13: Operational conditions for both the railway and people at the Dawlish seawall. The isolines corresponding to return period values of 5, 10, 25, 50, 100, 250 and 500 years are indicated.

303 Based on the pairs (η, H_{s0}) included in the isolines of the thresholds, we
304 can assess return periods associated to the different thresholds. The minimum
305 return period associated to the railway threshold is 163.5 years; whereas in
306 the case of people, this return period is 21.8 years. These results show that,
307 according to the thresholds specified by [66], combinations of wave and water
308 level events that could endanger the railway line located in the lee of the Dawlish
309 seawall are expected to occur, on average, every 163 years; whereas the people
310 (e.g., the maintenance workers of the railway lines) would be at risk, on average,
311 every 22 years.

312 4. Conclusions

313 In this work, a novel methodology to assess the operational conditions of
314 coastal infrastructures against flooding events is proposed. The methodology
315 was applied to a study case in the UK: the seawall in Dawlish, which is subjected
316 to recurrent overtopping and collapsed under the storm of February 2014. For
317 that, the joint probability of wave and water level data was analysed, and two
318 numerical models (SWAN and OpenFOAM[®]) were used to propagate waves and
319 compute overtopping discharges for thirty-six different combinations of water
320 level, significant wave height, and spectral peak period. These models were
321 validated through comparisons with wave buoy data and measurements collected
322 during laboratory experiments.

323 The results show that overtopping rates increase with both significant wave
324 height and water level. Among the thirty-six combinations tested, twenty-nine
325 generated non-zero wave overtopping discharges, twenty-two exceeded the oper-
326 ational limit proposed by the EurOtop for seawalls protecting people (0.3 l/s per
327 m) and eleven were greater than the EurOtop operational threshold for railway
328 lines in the lee of coastal structures (5 l/s per m). The maximum wave overtop-
329 ping discharge obtained was 16 l/s per m. To characterise the joint action of
330 the two main variables that drive wave overtopping (significant wave height and
331 water level), we defined a new variable: the *effective overtopping forcing*, which

332 was proven to explain 98% of the variability of the overtopping discharge.

333 The methodology was also applied to obtain the return periods associated
334 to the thresholds that limit the operational conditions for railway and people
335 uses. It was obtained that the minimum return period associated to the railway
336 (people) threshold is 163.5 years (21.8 years). Apart from these two specific
337 applications, the developed methodology could be used to compute the return
338 period associated with any other overtopping discharge value. In addition, it
339 could be applied to calculate the overtopping discharge induced by any sea state.
340 Thus, we can check if a certain coastal infrastructure is going to be operational
341 under any expected marine condition.

342 The composite methodology presented and applied in this work, which com-
343 prises advanced statistical techniques involving, laboratory experiments and two
344 different types of numerical models, is also extensible to other coastal regions
345 across the globe. It represents an advanced tool to assess the operational condi-
346 tions for different uses as well as to analyse the possible consequences of flooding
347 events on transport infrastructures and urban developments located in the lee
348 of coastal structures.

349 **Acknowledgements**

350 This work was carried out in the framework of the WAVEIMPACT Marie
351 Curie fellowship (PCIG-13-GA-2013-618556, European Commission, Marie Curie
352 fellowship, fellow GI) and the ICE project (Intelligent Community Energy, Eu-
353 ropean Commission, Contract no. 5025). CRD and RB were partly funded by
354 the University of Plymouth and the Spanish Ministry of Science, Innovation and
355 Universities (*Programa Juan de la Cierva 2017*, FJCI-2017-31781), respectively.

356 **References**

- 357 [1] A. Sperotto, S. Torresan, V. Gallina, E. Coppola, A. Critto, A. Marcomini,
358 A multi-disciplinary approach to evaluate pluvial floods risk under changing
359 climate: The case study of the municipality of Venice (Italy), *Science of the
360 Total Environment* 562 (2016) 1031–1043.
- 361 [2] S. Xian, J. Yin, N. Lin, M. Oppenheimer, Influence of risk factors and
362 past events on flood resilience in coastal megacities: Comparative analysis
363 of NYC and Shanghai, *Science of the Total Environment* 610 (2018) 1251–
364 1261.
- 365 [3] R. J. Bergillos, C. Rodriguez-Delgado, J. Allen, G. Iglesias, Wave energy
366 converter geometry for coastal flooding mitigation, *Science of the Total
367 Environment* 668 (2019) 1232–1241.
- 368 [4] J. Fang, D. Lincke, S. Brown, R. J. Nicholls, C. Wolff, J.-L. Merkens,
369 J. Hinkel, A. T. Vafeidis, P. Shi, M. Liu, Coastal flood risks in China
370 through the 21st century—An application of DIVA, *Science of the Total
371 Environment* (2019) 135311.
- 372 [5] A. G. Rumson, S. H. Hallett, Innovations in the use of data facilitating
373 insurance as a resilience mechanism for coastal flood risk, *Science of the
374 Total Environment* 661 (2019) 598–612.
- 375 [6] L. Vamvakeridou-Lyroudia, A. Chen, M. Khoury, M. Gibson, A. Kostaridis,
376 D. Stewart, M. Wood, S. Djordjevic, D. Savic, Assessing and visualising
377 hazard impacts to enhance the resilience of critical infrastructures to urban
378 flooding, *Science of The Total Environment* 707 (2020) 136078.
- 379 [7] T. Gallien, B. Sanders, R. Flick, Urban coastal flood prediction: Integrating
380 wave overtopping, flood defenses and drainage, *Coastal Engineering* 91
381 (2014) 18–28.

- 382 [8] T. Gallien, Validated coastal flood modeling at Imperial Beach, California:
383 Comparing total water level, empirical and numerical overtopping method-
384 ologies, *Coastal Engineering* 111 (2016) 95–104.
- 385 [9] D. Xie, Q.-P. Zou, A. Mignone, J. D. MacRae, Coastal flooding from wave
386 overtopping and sea level rise adaptation in the northeastern USA, *Coastal*
387 *Engineering* 150 (2019) 39–58.
- 388 [10] G. Iglesias, J. Abanades, Wave power - climate change mitigation and
389 adaptation, in: L. M. Chen W.-Y., Suzuki T. (Ed.), *Handbook of Climate*
390 *Change Mitigation and Adaptation*. Springer New York, p. 1-49, 2015.
- 391 [11] S. Muis, B. Güneralp, B. Jongman, J. C. Aerts, P. J. Ward, Flood risk
392 and adaptation strategies under climate change and urban expansion: A
393 probabilistic analysis using global data, *Science of the Total Environment*
394 538 (2015) 445–457.
- 395 [12] A. Sánchez-Arcilla, M. García-León, V. Gracia, R. Devoy, A. Stanica,
396 J. Gault, Managing coastal environments under climate change: Pathways
397 to adaptation, *Science of the Total Environment* 572 (2016) 1336–1352.
- 398 [13] J. Wang, S. Yi, M. Li, L. Wang, C. Song, Effects of sea level rise, land
399 subsidence, bathymetric change and typhoon tracks on storm flooding in
400 the coastal areas of Shanghai, *Science of the Total Environment* 621 (2018)
401 228–234.
- 402 [14] R. J. Bergillos, C. Rodriguez-Delgado, G. Iglesias, Wave farm impacts
403 on coastal flooding under sea-level rise: a case study in southern Spain,
404 *Science of the Total Environment* 653 (2019) 1522–1531.
- 405 [15] G. Bove, A. Becker, B. Sweeney, M. Vousdoukas, S. Kulp, A method for
406 regional estimation of climate change exposure of coastal infrastructure:
407 Case of USVI and the influence of digital elevation models on assessments,
408 *Science of The Total Environment* 710 (2020) 136162.

- 409 [16] A. Bomers, J. P. Aguilar Lopez, J. J. Warmink, S. J. M. H. Hulscher,
410 Modelling effects of an asphalt road at a dike crest on dike cover erosion
411 onset during wave overtopping, *Natural Hazards* (2018).
- 412 [17] T. Thieu Quang, H. Oumeraci, Numerical modelling of wave overtopping-
413 induced erosion of grassed inner sea-dike slopes, *Natural Hazards* 63 (2012)
414 417–447.
- 415 [18] J.-L. de Kok, M. Grossmann, Large-scale assessment of flood risk and the
416 effects of mitigation measures along the elbe river, *Natural Hazards* 52
417 (2010) 143–166.
- 418 [19] H. T. Le, H. J. Verhagen, J. K. Vrijling, Damage to grass dikes due to wave
419 overtopping, *Natural Hazards* 86 (2017) 849–875.
- 420 [20] F. Chiganne, C. Marche, T.-F. Mahdi, Evaluation of the overflow failure
421 scenario and hydrograph of an embankment dam with a concrete upstream
422 slope protection, *Natural Hazards* 71 (2014) 21–39.
- 423 [21] S.-J. Wu, J.-C. Yang, Y.-K. Tung, Risk analysis for flood-control structure
424 under consideration of uncertainties in design flood, *Natural Hazards* 58
425 (2011) 117–140.
- 426 [22] A. Y. Hoekstra, J.-L. De Kok, Adapting to climate change: a comparison
427 of two strategies for dike heightening, *Natural Hazards* 47 (2008) 217–228.
- 428 [23] Q. Zhong, W. Wu, S. Chen, M. Wang, Comparison of simplified physically
429 based dam breach models, *Natural Hazards* 84 (2016) 1385–1418.
- 430 [24] N. Javadi, T.-F. Mahdi, Experimental investigation into rockfill dam failure
431 initiation by overtopping, *Natural Hazards* 74 (2014) 623–637.
- 432 [25] D. Vicinanza, I. Cáceres, M. Buccino, X. Gironella, M. Calabrese, Wave
433 disturbance behind low-crested structures: Diffraction and overtopping ef-
434 fects, *Coastal Engineering* 56 (2009) 1173–1185.

- 435 [26] C. Iuppa, L. Cavallaro, R. E. Musumeci, D. Vicinanza, E. Foti, Empirical
436 cal overtopping volume statistics at an OBREC, *Coastal Engineering* 152
437 (2019) 103524.
- 438 [27] A. J. Evans, B. Garrod, L. B. Firth, S. J. Hawkins, E. S. Morris-Webb,
439 H. Goudge, P. J. Moore, Stakeholder priorities for multi-functional coastal
440 defence developments and steps to effective implementation, *Marine Policy*
441 75 (2017) 143 – 155.
- 442 [28] Q. Yu, A. K. H. Lau, K. T. Tsang, J. C. H. Fung, Human damage as-
443 sessments of coastal flooding for hong kong and the pearl river delta due
444 to climate change-related sea level rise in the twenty-first century, *Natural*
445 *Hazards* 92 (2018) 1011–1038.
- 446 [29] S. F. Silva, M. Martinho, R. Capito, T. Reis, C. J. Fortes, J. C. Ferreira,
447 An index-based method for coastal-flood risk assessment in low-lying areas
448 (costa de caparica, portugal), *Ocean & Coastal Management* 144 (2017)
449 90 – 104.
- 450 [30] Y. Fang, J. Yin, B. Wu, Flooding risk assessment of coastal tourist attrac-
451 tions affected by sea level rise and storm surge: a case study in zhejiang
452 province, china, *Natural Hazards* 84 (2016) 611–624.
- 453 [31] T. Gallien, W. O’Reilly, R. Flick, R. Guza, Geometric properties of an-
454 thropogenic flood control berms on southern California beaches, *Ocean &*
455 *Coastal Management* 105 (2015) 35 – 47.
- 456 [32] P. Bernatchez, C. Fraser, D. Lefaiivre, S. Dugas, Integrating anthropogenic
457 factors, geomorphological indicators and local knowledge in the analysis of
458 coastal flooding and erosion hazards, *Ocean & Coastal Management* 54
459 (2011) 621 – 632.
- 460 [33] M. P. Bunicontro, S. C. Marcomini, R. A. López, The effect of coastal
461 defense structures (mounds) on southeast coast of Buenos Aires province,
462 Argentina, *Ocean & Coastal Management* 116 (2015) 404 – 413.

- 463 [34] A. Carrasco, Ó. Ferreira, A. Matias, P. Freire, Flood hazard assessment
464 and management of fetch-limited coastal environments, *Ocean & Coastal*
465 *Management* 65 (2012) 15 – 25.
- 466 [35] N. P. Kurian, N. Nirupama, M. Baba, K. V. Thomas, Coastal flooding
467 due to synoptic scale, meso-scale and remote forcings, *Natural Hazards* 48
468 (2009) 259–273.
- 469 [36] I.-J. Moon, I. S. Oh, T. Murty, Y.-H. Youn, Causes of the unusual coastal
470 flooding generated by typhoon winnie on the west coast of korea, *Natural*
471 *Hazards* 29 (2003) 485–500.
- 472 [37] J. Geeraerts, P. Troch, J. De Rouck, H. Verhaeghe, J. J. Bouma, Wave over-
473 topping at coastal structures: prediction tools and related hazard analysis,
474 *Journal of Cleaner Production* 15 (2007) 1514–1521.
- 475 [38] H. Schüttrumpf, H. Oumeraci, Layer thicknesses and velocities of wave
476 overtopping flow at seadikes, *Coastal Engineering* 52 (2005) 473 – 495.
- 477 [39] T. Suzuki, C. Altomare, W. Veale, T. Verwaest, K. Trouw, P. Troch, M. Zi-
478 jlema, Efficient and robust wave overtopping estimation for impermeable
479 coastal structures in shallow foreshores using SWASH, *Coastal Engineering*
480 122 (2017) 108 – 123.
- 481 [40] C. Coelho, T. Cruz, P. Roebeling, Longitudinal revetments to mitigate
482 overtopping and flooding: Effectiveness, costs and benefits, *Ocean &*
483 *Coastal Management* 134 (2016) 93 – 102.
- 484 [41] B. Renard, M. Lang, Use of a Gaussian copula for multivariate extreme
485 value analysis: Some case studies in hydrology, *Advances in Water Re-*
486 *sources* 30 (2007) 897 – 912.
- 487 [42] J. A. Tawn, Bivariate extreme value theory: Models and estimation,
488 *Biometrika* 75 (1988) 397–415.

- 489 [43] I. Morton, J. Bowers, Extreme value analysis in a multivariate offshore
490 environment, *Applied Ocean Research* 18 (1996) 303 – 317.
- 491 [44] M. Kramer, B. Zanuttigh, J. Van der Meer, C. Vidal, F. Gironella, Lab-
492 oratory experiments on low-crested breakwaters, *Coastal Engineering* 52
493 (2005) 867–885.
- 494 [45] S. A. Hughes, N. Nadal, Laboratory study of combined wave overtopping
495 and storm surge overflow of a levee, *Coastal Engineering* 56 (2009) 244–259.
- 496 [46] T. Pullen, W. Allsop, T. Bruce, J. Pearson, Field and laboratory measure-
497 ments of mean overtopping discharges and spatial distributions at vertical
498 seawalls, *Coastal Engineering* 56 (2009) 121–140.
- 499 [47] J. W. van der Meer, H. Verhaeghe, G. J. Steendam, The new wave over-
500 topping database for coastal structures, *Coastal Engineering* 56 (2009) 108
501 – 120. The CLASH Project.
- 502 [48] D. Gallach-Sánchez, P. Troch, T. Vroman, L. Pintelon, A. Kortenhaus,
503 Experimental study of overtopping performance of steep smooth slopes for
504 shallow water wave conditions, in: *Proceedings of the 5th Conference*
505 *on the Application of Physical Modelling to Port and Coastal Protection*
506 *(Coastlab14)*. Varna, Bulgaria, 2014.
- 507 [49] Y. Pan, C. Kuang, L. Li, F. Amini, Full-scale laboratory study on distri-
508 bution of individual wave overtopping volumes over a levee under negative
509 freeboard, *Coastal Engineering* 97 (2015) 11–20.
- 510 [50] C. Iuppa, P. Contestabile, L. Cavallaro, E. Foti, D. Vicinanza, Hydraulic
511 performance of an innovative breakwater for overtopping wave energy con-
512 version, *Sustainability* 8 (2016) 1226.
- 513 [51] M. Salauddin, J. Pearson, Laboratory investigation of overtopping at a
514 sloping structure with permeable shingle foreshore, *Ocean Engineering* 197
515 (2020) 106866.

- 516 [52] X. Chen, B. Hofland, C. Altomare, T. Suzuki, W. Uijttewaal, Forces on a
517 vertical wall on a dike crest due to overtopping flow, *Coastal Engineering*
518 95 (2015) 94 – 104.
- 519 [53] K. Pillai, A. Etemad-Shahidi, C. Lemckert, Wave overtopping at berm
520 breakwaters: Experimental study and development of prediction formula,
521 *Coastal Engineering* 130 (2017) 85–102.
- 522 [54] K. V. Doorslaer, A. Romano, J. D. Rouck, A. Kortenhaus, Impacts on a
523 storm wall caused by non-breaking waves overtopping a smooth dike slope,
524 *Coastal Engineering* 120 (2017) 93 – 111.
- 525 [55] J. Molines, J. R. Medina, Calibration of overtopping roughness factors
526 for concrete armor units in non-breaking conditions using the CLASH
527 database, *Coastal Engineering* 96 (2015) 62 – 70.
- 528 [56] B. Zanuttigh, S. M. Formentin, J. W. van der Meer, Prediction of extreme
529 and tolerable wave overtopping discharges through an advanced neural net-
530 work, *Ocean Engineering* 127 (2016) 7–22.
- 531 [57] J. Molines, M. P. Herrera, J. R. Medina, Estimations of wave forces on
532 crown walls based on wave overtopping rates, *Coastal Engineering* 132
533 (2018) 50 – 62.
- 534 [58] J. Molines, M. P. Herrera, M. E. Gómez-Martín, J. R. Medina, Distribution
535 of individual wave overtopping volumes on mound breakwaters, *Coastal*
536 *Engineering* 149 (2019) 15–27.
- 537 [59] C. Altomare, T. Suzuki, X. Chen, T. Verwaest, A. Kortenhaus, Wave
538 overtopping of sea dikes with very shallow foreshores, *Coastal Engineering*
539 116 (2016) 236 – 257.
- 540 [60] N. Kobayashi, A. Farhadzadeh, J. Melby, B. Johnson, M. Gravens, Wave
541 overtopping of levees and overwash of dunes, *Journal of Coastal Research*
542 (2010) 888–900.

- 543 [61] K. Hu, C. Mingham, D. Causon, Numerical simulation of wave overtopping
544 of coastal structures using the non-linear shallow water equations, *Coastal*
545 *Engineering* 41 (2000) 433 – 465.
- 546 [62] S. Shao, C. Ji, D. I. Graham, D. E. Reeve, P. W. James, A. J. Chadwick,
547 Simulation of wave overtopping by an incompressible SPH model, *Coastal*
548 *Engineering* 53 (2006) 723 – 735.
- 549 [63] M. J. Wesley, K. F. Cheung, Modeling of wave overtopping on vertical
550 structures with the HLLS Riemann solver, *Coastal Engineering* 112 (2016)
551 28 – 43.
- 552 [64] C. Hirt, B. Nichols, Volume of fluid (VOF) method for the dynamics of
553 free boundaries, *Journal of Computational Physics* 39 (1981) 201 – 225.
- 554 [65] L. Franco, M. de Gerloni, J. van der Meer, Wave overtopping at vertical
555 and composite breakwaters, *Proc. 24th ICCE, Kobe, October 23-28, 1994*
556 (1994).
- 557 [66] J. Van der Meer, N. Allsop, T. Bruce, J. De Rouck, A. Kortenhaus,
558 T. Pullen, H. Schüttrumpf, P. Troch, B. Zanuttigh, EurOtop, Manual on
559 wave overtopping of sea defences and related structures. An overtopping
560 manual largely based on European research, but for worldwide application,
561 Technical Report, 2018.
- 562 [67] T. Petroliaqkis, E. Voukouvalas, J. Disperati, J. Bidlot, Joint probabilities
563 of storm surge, significant wave height and river discharge components
564 of coastal flooding events, *European Commission-JRC Technical Reports*
565 (2016).
- 566 [68] L. Holthuijsen, N. Booij, R. Ris, A spectral wave model for the coastal
567 zone, ASCE, 1993.
- 568 [69] N. Booij, R. C. Ris, L. H. Holthuijsen, A third-generation wave model for
569 coastal regions: 1. Model description and validation, *Journal of Geophysical*
570 *Research: Oceans* 104 (1999) 7649–7666.

- 571 [70] R. J. Bergillos, A. López-Ruiz, M. Ortega-Sánchez, G. Masselink, M. A.
572 Losada, Implications of delta retreat on wave propagation and longshore
573 sediment transport-Guadalefo case study (southern Spain), *Marine Geol-*
574 *ogy* 382 (2016) 1–16.
- 575 [71] R. J. Bergillos, G. Masselink, R. T. McCall, M. Ortega-Sánchez, Mod-
576 elling overwash vulnerability along mixed sand-gravel coasts with XBeach-
577 G: Case study of Playa Granada, southern Spain, in: *Coastal Engineering*
578 *Proceedings*, volume 1 (35), 2016, p. 13.
- 579 [72] A. López-Ruiz, R. J. Bergillos, M. Ortega-Sánchez, The importance of
580 wave climate forecasting on the decision-making process for nearshore wave
581 energy exploitation, *Applied energy* 182 (2016) 191–203.
- 582 [73] A. López-Ruiz, R. J. Bergillos, M. Ortega-Sánchez, M. A. Losada, Impact of
583 river regulation on the submerged morphology of a Mediterranean deltaic
584 system: evaluating Coastal Engineering tools, in: *Coastal Engineering*
585 *Proceedings*, volume 1 (35), 2016, p. 10.
- 586 [74] R. J. Bergillos, C. Rodríguez-Delgado, M. Ortega-Sánchez, Advances in
587 management tools for modeling artificial nourishments in mixed beaches,
588 *Journal of Marine Systems* 172 (2017) 1–13.
- 589 [75] R. J. Bergillos, G. Masselink, M. Ortega-Sánchez, Coupling cross-shore
590 and longshore sediment transport to model storm response along a mixed
591 sand-gravel coast under varying wave directions, *Coastal Engineering* 129
592 (2017) 93–104.
- 593 [76] R. J. Bergillos, A. López-Ruiz, D. Principal-Gómez, M. Ortega-Sánchez, An
594 integrated methodology to forecast the efficiency of nourishment strategies
595 in eroding deltas, *Science of the Total Environment* 613 (2018) 1175–1184.
- 596 [77] R. J. Bergillos, A. Lopez-Ruiz, E. Medina-Lopez, A. Monino, M. Ortega-
597 Sanchez, The role of wave energy converter farms on coastal protection in

- 598 eroding deltas, Guadalfeo, southern Spain, *Journal of Cleaner Production*
599 171 (2018) 356–367.
- 600 [78] A. López-Ruiz, R. J. Bergillos, J. M. Raffo-Caballero, M. Ortega-Sánchez,
601 Towards an optimum design of wave energy converter arrays through an
602 integrated approach of life cycle performance and operational capacity, *Ap-
603 plied Energy* 209 (2018) 20–32.
- 604 [79] A. López-Ruiz, R. J. Bergillos, A. Lira-Loarca, M. Ortega-Sánchez, A
605 methodology for the long-term simulation and uncertainty analysis of the
606 operational lifetime performance of wave energy converter arrays, *Energy*
607 153 (2018) 126–135.
- 608 [80] P. Magaña, R. J. Bergillos, J. Del-Rosal-Salido, M. A. Reyes-Merlo, P. Díaz-
609 Carrasco, M. Ortega-Sánchez, Integrating complex numerical approaches
610 into a user-friendly application for the management of coastal environ-
611 ments, *Science of the Total Environment* 624 (2018) 979–990.
- 612 [81] C. Rodriguez-Delgado, R. J. Bergillos, M. Ortega-Sánchez, G. Iglesias, Pro-
613 tection of gravel-dominated coasts through wave farms: Layout and shore-
614 line evolution, *Science of The Total Environment* 636 (2018) 1541–1552.
- 615 [82] C. Rodriguez-Delgado, R. J. Bergillos, M. Ortega-Sánchez, G. Iglesias,
616 Wave farm effects on the coast: The alongshore position, *Science of the
617 Total Environment* 640 (2018) 1176–1186.
- 618 [83] C. Rodriguez-Delgado, R. J. Bergillos, G. Iglesias, Dual wave energy con-
619 verter farms and coastline dynamics: the role of inter-device spacing, *Sci-
620 ence of the Total Environment* 646 (2019) 1241–1252.
- 621 [84] R. J. Bergillos, C. Rodriguez-Delgado, J. Allen, G. Iglesias, Wave energy
622 converter configuration in dual wave farms, *Ocean Engineering* 178 (2019)
623 204–214.

- 624 [85] C. Rodriguez-Delgado, R. J. Bergillos, G. Iglesias, Dual wave farms for
625 energy production and coastal protection under sea level rise, *Journal of*
626 *Cleaner Production* 222 (2019) 364–372.
- 627 [86] C. Rodriguez-Delgado, R. J. Bergillos, G. Iglesias, An artificial neural
628 network model of coastal erosion mitigation through wave farms, *Environ-*
629 *mental Modelling and Software* 119 (2019) 390–399.
- 630 [87] H. G. Weller, G. Tabor, H. Jasak, C. Fureby, A tensorial approach to com-
631 putational continuum mechanics using object-oriented techniques, *Com-*
632 *puters in Physics* 12 (1998) 620–631.
- 633 [88] D. Dawson, J. Shaw, W. R. Gehrels, Sea-level rise impacts on transport
634 infrastructure: The notorious case of the coastal railway line at Dawlish,
635 England, *Journal of Transport Geography* 51 (2016) 97 – 109.
- 636 [89] C. G. Soares, M. Scotto, Application of the r largest-order statistics for
637 long-term predictions of significant wave height, *Coastal Engineering* 51
638 (2004) 387 – 394.